

## Introduction

This document provides additional results, more detail on the calculations and thermodynamical data used in the calculations with some of the models.

### S1 Additional results

- 5 The following sections contains the variations of supersaturation, surface tensions and the organic bulk–surface partitioning factors along Köhler curves predicted with the different models for particles of succinic and glutaric acids mixed with ammonium sulphate. Table S1 contains properties of the organic acids as pure compounds including molar mass, density in solid phase, density and surface tension in a hypothetical supercooled liquid state. The results presented here are for with dry particle size of  $D_p = 50$  nm at organic mass fractions ( $w_{p,org}$ ) of 0.2, 0.5, 0.8 and 0.95 all at 298.15 K for all the different model
- 10 calculations. A sensitivity analysis regarding the compressed film model at  $w_{p,org} = 0.95$  is also provided due to the second local maxima visible in the Köhler curves of the three acids investigated.

#### S1.1 Succinic acid

Table S2 shows the droplet properties at the critical point (diameter, surface tension and supersaturation) predicted with different models in the case of succinic acid–ammonium sulphate particles.

- 15 Figure S1 shows the Köhler curves predicted with the different models for particles containing succinic acid. These results show similar trends to those of malonic acid. In Figs. S1(c) and S1(d), the curve predicted with the partial organic film model shows a larger discrepancy after the surface coverage of the organic film becomes partial compared to the curves predicted with the monolayer, Gibbs and bulk solution models than it did with the curve predicted for particles containing malonic acid. The discrepancy is still not large.

- 20 Figure S2 shows the surface tensions predicted with the different partitioning models along the Köhler curves for simulations with succinic acid. These results are similar in appearance and behavior to those of malonic acid.

- Figure S3 shows the organic surface partitioning factors predicted with the different models for the simulations with succinic acid. These results show similar trends to those of malonic acid. Aside from the differences in the shape of the curves and intersection point between the curves predicted with the monolayer and Gibbs models, the main difference is that at low
- 25 organic mass fraction in Fig. S3(a), the monolayer model predicts considerably stronger partitioning at small droplet sizes than in the case with malonic acid. In addition, the partitioning predicted with the Gibbs model becomes stronger compared to the monolayer model even in Fig. S3(a), something that does not occur with malonic acid.

#### S1.2 Glutaric acid

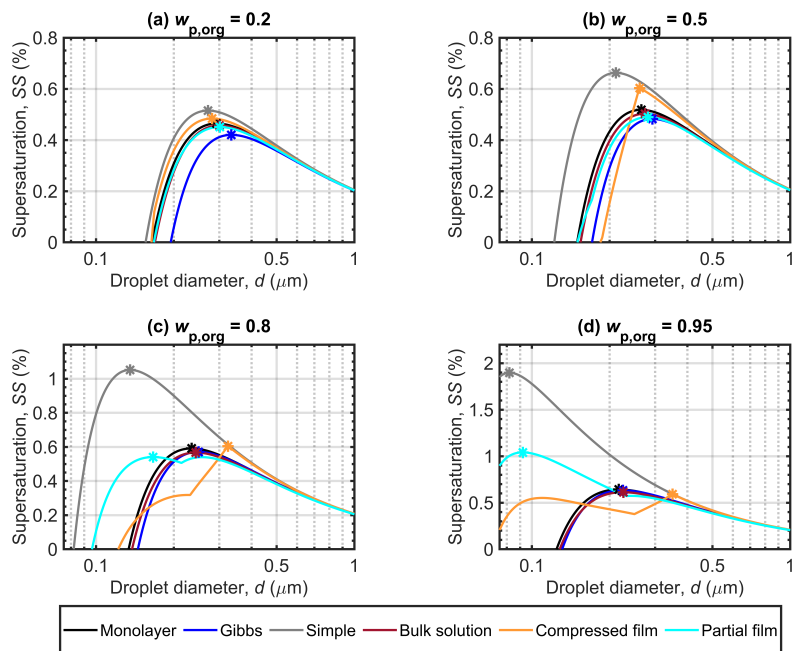
- Table S3 shows the droplet properties at the critical point (diameter, surface tension and supersaturation) predicted with different
- 30 models in the case of glutaric acid–ammonium sulphate particles.

Figure S4 shows the Köhler curves predicted with the different models for particles containing glutaric acid. The overall behavior of the curves show similar trends to those observed in the simulations with the other two compounds. In Figs. S4(c)

**Table S1.** The molar masses ( $M$ ), liquid and solid densities ( $\rho_L$  and  $\rho_S$ ) and surface tensions ( $\sigma$ ) of succinic and glutaric acids at 298.15 K, unless stated otherwise.

Compound	$M$ (g mol <sup>-1</sup> )	$\rho_L$ (kg m <sup>-3</sup> )	$\rho_S$ (kg m <sup>-3</sup> )	$\sigma$ (mN m <sup>-1</sup> )
Succinic acid	118.089	1470.73 <sup>a</sup>	1572.0 <sup>b</sup>	47.67 <sup>c</sup>
Glutaric acid	132.116	1274.48 <sup>d</sup>	1429.0 <sup>b</sup> (288.15 K)	50.76 <sup>e</sup>

<sup>a</sup> Hyvärinen et al. (2006) <sup>b</sup> CRC Handbook (1988) <sup>c</sup> Vanhanen et al. (2008) <sup>d</sup> Extended from Cai et al. (2015), <sup>e</sup> Extended from binary fit based on measurements by Bzdek et al. (2016)



**Figure S1.** Köhler curves calculated with the different partitioning models for dry succinic acid–ammonium sulphate particles with  $D_p = 50$  nm. Each panel shows curves for particles with a different succinic acid mass fraction ( $w_{p,org}$ ). The critical points are marked on each curve. Note that the vertical axis scaling changes between the panels.

**Table S2.** The critical droplet diameters ( $d_c$ ), supersaturations ( $SS_c$ ) and surface tensions ( $\sigma_c$ ) predicted with the different models in simulations for mixed succinic acid–ammonium sulfate particles of  $D_p = 50$  nm at 298.15 K.

Parameter	$d_c$ (nm)	$SS_c$ (%)	$\sigma_c$ (mN m <sup>-1</sup> )	$d_c$ (nm)	$SS_c$ (%)	$\sigma_c$ (mN m <sup>-1</sup> )	$d_c$ (nm)	$SS_c$ (%)	$\sigma_c$ (mN m <sup>-1</sup> )	
$w_{p,org}$	Monolayer			Gibbs			Simple			
	0.2	292.82	0.46	71.16	333.98	0.42	71.4	271.19	0.52	71.97
	0.5	265.31	0.52	70.32	292.82	0.48	70.66	211.54	0.66	71.97
	0.8	234.32	0.59	69.47	249.34	0.57	69.72	135.46	1.05	71.97
0.95	217.02	0.64	69.02	225.09	0.63	69.15	81.82	1.9	71.97	
$w_{p,org}$	Bulk solution			Compressed film			Partial organic film			
	0.2	300.4	0.46	71.07	281.28	0.48	71.97	301.5	0.45	68.71
	0.5	274.18	0.5	70.26	261.46	0.6	71.97	281.28	0.49	62.77
	0.8	243.04	0.57	69.46	324.36	0.6	71.97	166.22	0.54	47.67
	0.95	225.92	0.61	69.04	350.22	0.59	71.97	92.31	1.04	47.67

and S4(d), the curve predicted with the partial organic film model after the film breaks and the group of monolayer, Gibbs and bulk model curves do not match as well as in the case of the malonic acid simulations. This behavior is similar to Fig. S1 with the succinic acid simulations. In addition, it appears that with the glutaric acid simulation, the curve predicted with the compressed film model intercepts the partial organic film curve very near the point of the surface film breaking in the case of Figs. S4(b), S4(c) and S4(d). As this does not happen with the other test systems, it may be an insignificant detail.

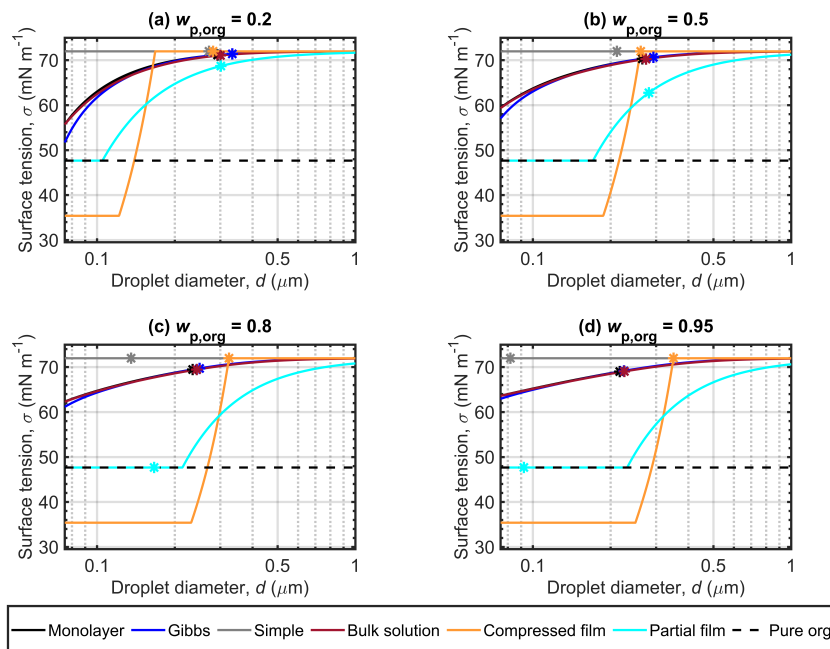


**Figure S2.** Surface tensions of droplets along the Köhler curves, calculated with the different partitioning models for dry particles of  $D_p = 50$  nm at different succinic acid mass fractions ( $w_{p,org}$ ) in the different panels. The critical points evaluated for the Köhler curves in Fig. S1 are also marked, and the surface tension of pure succinic acid estimated according to Vanhanen et al. (2008) is indicated as a physical lower limit for the droplet surface tension.

**Table S3.** The critical droplet diameters ( $d_c$ ), supersaturations ( $SS_c$ ) and surface tensions ( $\sigma_c$ ) predicted with the different models in simulations for mixed glutaric acid–ammonium sulfate particles of  $D_p = 50$  nm at 298.15 K.

Parameter	$d_c$ (nm)	$SS_c$ (%)	$\sigma_c$ ( $\text{mN m}^{-1}$ )	$d_c$ (nm)	$SS_c$ (%)	$\sigma_c$ ( $\text{mN m}^{-1}$ )	$d_c$ (nm)	$SS_c$ (%)	$\sigma_c$ ( $\text{mN m}^{-1}$ )
$w_{p,org}$	Monolayer			Gibbs			Simple		
0.2	288.57	0.47	71.37	329.13	0.43	71.57	268.24	0.52	71.97
0.5	253.93	0.54	70.49	278.22	0.51	70.89	206.2	0.68	71.97
0.8	219.41	0.63	69.13	226.74	0.63	69.54	131.08	1.09	71.97
0.95	199.53	0.7	68.1	200.26	0.72	68.34	80.05	1.96	71.97
$w_{p,org}$	Bulk solution			Compressed film			Partial organic film		
0.2	292.82	0.47	71.31	278.22	0.49	71.97	298.22	0.46	68.68
0.5	262.42	0.53	70.44	216.23	0.64	71.97	274.18	0.5	62.71
0.8	230.92	0.61	69.17	264.35	0.72	71.83	154.5	0.62	50.76
0.95	213.09	0.66	68.27	284.38	0.73	71.97	87.7	1.18	50.76

Figure S5 shows the surface tensions predicted with the different models along the Köhler curves for particles containing glutaric acid. The results again show similar trends to the other compounds. Figs. S5(b), S5(c) and S5(d) show that the predicted surface tension curves of the compressed film model and partial organic film intercept near the point where the organic film breaks in the latter model. This does not happen with the other two compounds. Table S3 shows that in Fig. S5(c),  $\sigma_c$  of the

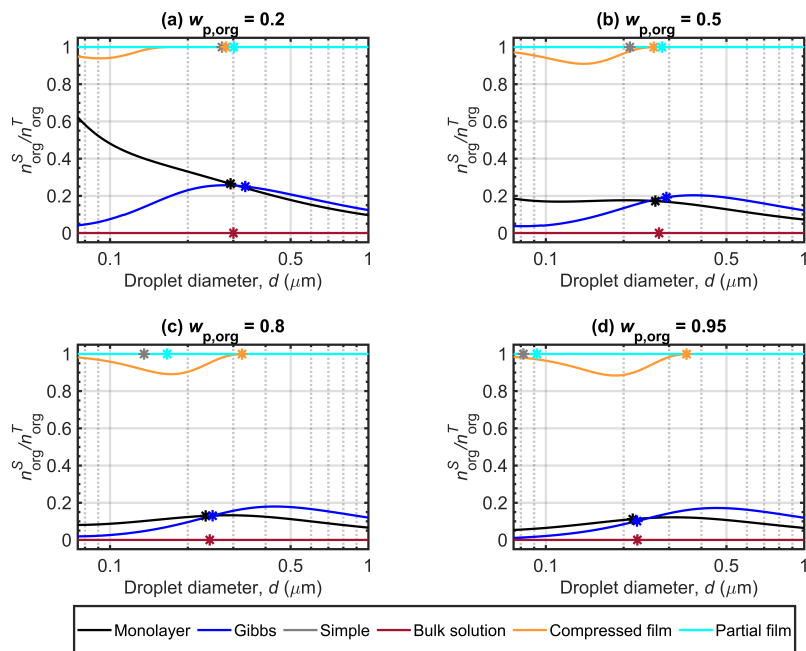


**Figure S3.** Succinic acid surface partitioning factors ( $n_{\text{org}}^S/n_{\text{org}}^B$ ) predicted with the different models along the Köhler curves for dry particles with  $D_p = 50$  nm at different organic mass fractions ( $w_{p,\text{org}}$ ) in the different panels. The critical points are also marked.

predicted surface tension with compressed film model is slightly below that of pure water. There is no clear indication why this happens and could be due to some numerical glitch.

- Figure S6 shows the organic surface partitioning factor for the different models for the simulations with glutaric acid. Notably, the partitioning predicted with the Gibbs model is noticeably stronger than for the other two acids. This is also true for the monolayer model predictions though to a smaller degree. In addition, the compressed film model has a partitioning factor practically equal to unity the whole time, the minimum value out of all organic mass fractions is 0. 0.9984 for  $w_{p,\text{org}} = 0.95$  simulation.

### S1.3 Surface thickness

- Figure S7 shows the monolayer thickness modeled with the monolayer model of Malila and Prisle (2018) at different organic mass fractions ( $w_{p,\text{org}}$ ) for malonic, succinic and glutaric acids. At the point of activation, the predicted surface thickness is 0.39 - 0.4 nm for all acids.

## S2 Calculation details

- The following sections contain details relating to the calculation of initial amounts of salt, organic and water as well as activity, surface tension and density.

### S2.1 Initial amount of organic and salt molecules

Initial amount of organic and salt molecules are calculated with the assumption of spherical particles ( $V_p = \frac{\pi}{6} D_p^3$ ) and additive solid phase volumes. Starting from the definition of the organic mass fraction ( $w_{p,\text{org}}$ ), the relation between the initial salt and

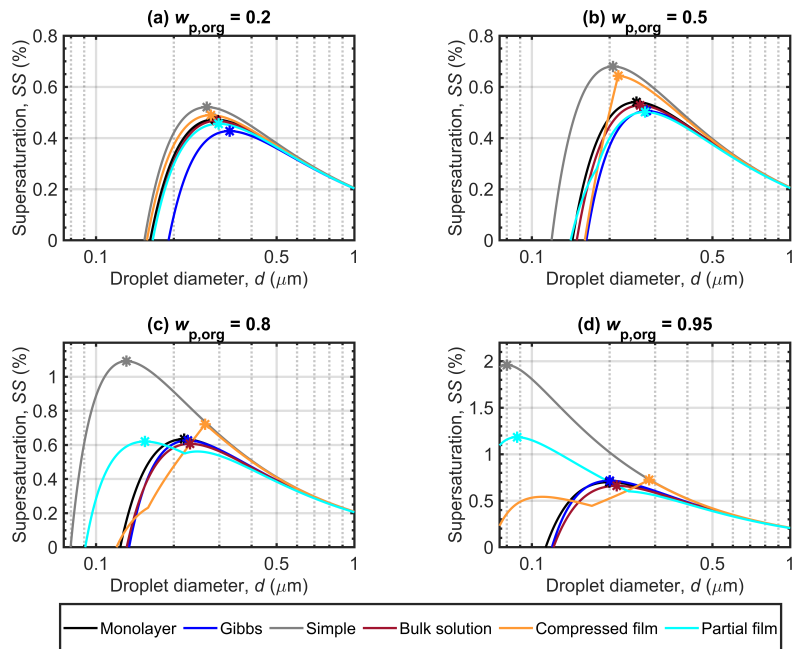


**Figure S4.** Köhler curves calculated with the different partitioning models for dry glutaric acid–ammonium sulphate particles with  $D_p = 50$  nm. Each panel shows curves for particles with a different glutaric acid mass fraction ( $w_{p,org}$ ). The critical points are marked on each curve. Note that the vertical axis scaling changes between the panels.

organic mass in the particle can be solved as

$$60 \quad m_{\text{salt}}^i = \frac{(1 - w_{p,org})m_{\text{org}}^i}{w_{p,org}}. \quad (\text{S1})$$

The initial mass of organic in the particle can be derived starting with the basic equation  $m_{\text{org}}^i = V_{\text{org}}\rho_{\text{org}}^i$ . Solving for  $V_{\text{org}}$  and substituting it in terms of volume fraction and the particle volume, and then writing out the volume fraction in terms of initial masses and densities and making use of Eq. (S1) finally leads the equation for the initial the organic mass

$$m_{\text{org}}^i = \frac{V_p}{\frac{1}{\rho_{\text{org}}^s} + \frac{(1-w_{p,org})}{w_{p,org}\rho_{\text{salt}}^s}}. \quad (\text{S2})$$

65 The initial amounts of molecules can then be calculated by dividing Eqs. (S1) and (S2) with the corresponding molecular mass  $m_j = M_j/N_A$ .

The compressed film model (Ruehl et al., 2016) employs different equations but with the same assumptions (see Ruehl et al. (2016) supplement), using a salt seed particle covered by an organic layer.

## S2.2 Initial amount of water molecules

70 Calculations with the assumption of additive volumes of the dry particle and of the water condensed on it follow equation (or a similar equivalent one)

$$n_w^T = \frac{\rho_w}{M_w} \frac{\pi}{6} (d^3 - D_p^3) N_A, \quad (\text{S3})$$

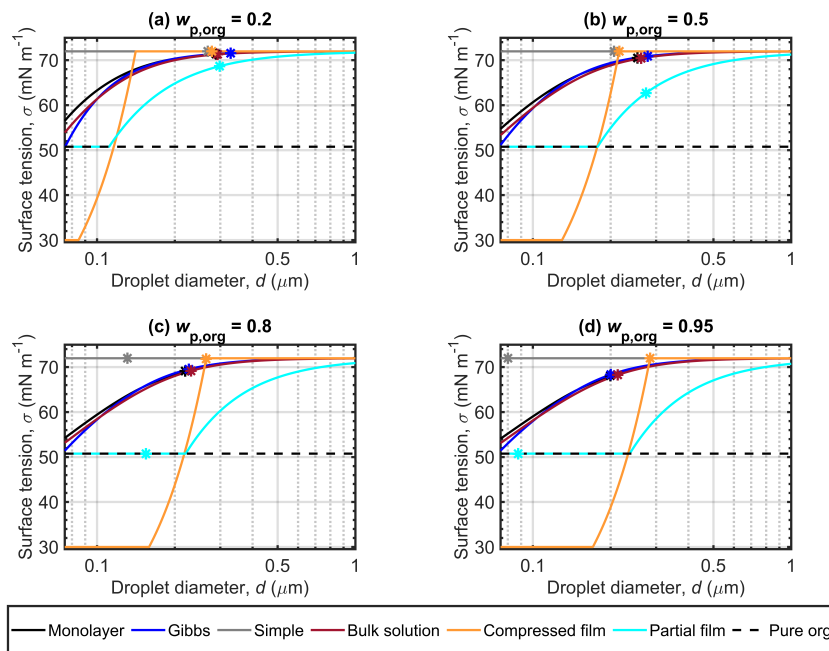


**Figure S5.** Surface tensions of droplets along the Köhler curves, calculated with the different partitioning models for dry particles of  $D_p = 50$  nm at different glutaric acid mass fractions ( $w_{p,org}$ ) in the different panels. The critical points evaluated for the Köhler curves in Fig. S4 are also marked, and the surface tension of pure glutaric acid estimated though extending the binary fit of Bzdek et al. (2016) is indicated as a physical lower limit for the droplet surface tension.

where  $\rho_w$  is the density of water,  $M_w$  the molar mass of water,  $d$  the droplet diameter,  $D_p$  the dry particle diameter and  $N_A$  Avogadro's number.

75 For the iterative method based on mass conservation using the solution density, the following equation

$$\left| \frac{\pi}{6} d^3 \rho(x, T) - n_w^T m_w - n_{org}^T m_{org} - n_{salt}^T m_{salt} \right| = 0 \quad (S4)$$

is solved for  $n_w^T$  using Matlab function *fsolve* where  $\rho$  is the composition dependant liquid solution density,  $x$  is a mole fraction matrix containing water, organic and salt and  $m_j$  is the molecular mass of compound  $j$  (water, organic, salt). Whatever moles or the number of molecules are used for calculations varies between the models.

## 80 S2.3 Water activity

The ideal water activity is calculated as the corrected mole fraction according to equation

$$a_w = \frac{n_w}{n_w + i_{salt} n_{salt} + i_{org} n_{org}}, \quad (S5)$$

where  $n_w$ ,  $n_{salt}$  and  $n_{org}$  are the number of molecules of water, salt and organic,  $i_{salt}$  is the van't Hoff factor for salt, and  $i_{org}$  for the organic. In the case of ammonium sulphate, the van't Hoff factor is calculated as

$$85 \quad i_{salt} = \max(-0.007931 (\ln b_{salt})^2 - 0.1844 \ln b_{salt} + 1.9242, 1.9242) \quad (S6)$$

where  $b_{salt}$  is the molality of ammonium sulfate. The equation has been restricted in case of molality values outside of the region it was intended for (Young and Warren, 1992). For the organic, van't Hoff factors equal to unity are assumed.

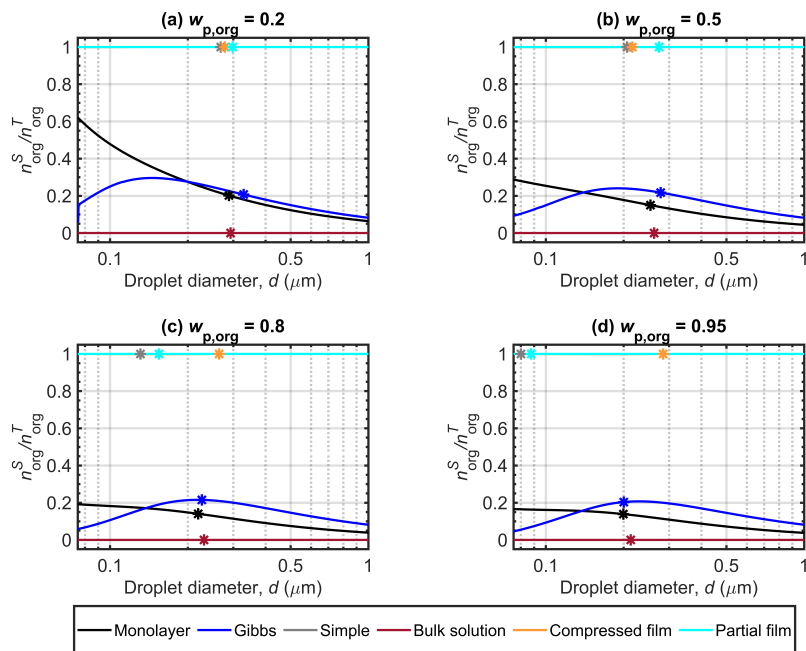


**Figure S6.** Glutaric acid surface partitioning factors ( $n_{\text{org}}^S/n_{\text{org}}^T$ ) predicted with the different models along the Köhler curves for dry particles with  $D_p = 50$  nm at different organic mass fractions ( $w_{p,\text{org}}$ ) in the different panels. The critical points are also marked.

For the binary systems of salt (ammonium sulphate) and water, the Prisle (2006) fit used for the simple model (Prisle et al., 2011) gives the activity as

$$90 \quad a_w = 1 - 0.039767b_{\text{salt}} + 0.0079808b_{\text{salt}}^2 - 0.0022641b_{\text{salt}}^3. \quad (\text{S7})$$

The water activity can then be calculated as  $a_w = x_w \gamma_w$ . The AIOMFAC based (AIOMFAC-web) fit used for the partial organic film model (Ovadnevaite et al., 2017) is

$$a_w = 0.0011 \cdot \exp(-7.0930 \cdot 10^2 \cdot x_{\text{salt}}) + 0.9989 \cdot \exp(-1.8762 \cdot x_{\text{salt}}) \quad (\text{S8})$$

where  $x_{\text{salt}}$  is the mole fraction of ammonium sulphate. The fit was done at 298.15K.

## 95 S2.4 Compressed film model parameters and sensitivity analysis

Table S4 contains the model parameters used for the calculations with the compressed film model of Ruehl et al. (2016). This study does not contain new fittings of the parameters. However, it should be noted that when fitting the parameters, the properties of growing droplets are quite different at lower sub-saturation RH values and near the critical point. For good parameters, one should have data at sufficiently high supersaturation making such data somewhat difficult to acquire as all

100  $D_{\text{seed}}$ ,  $D_p$  and  $d$  are needed in addition to the RH. The fitting happens to the droplet sizes before activation (the rising part of the Köhler curve) at one organic fraction like Ruehl et al. (2016), or across several organic fractions at one RH value like Forestieri et al. (2018). Assuming that the parameters are physical constants, they can be applied to a range of conditions.

105 For all the compounds, at  $w_{p,\text{org}} = 0.95$  there is a second local maxima visible in the predicted Köhler curves (Figs. 1, S1 S4) that is sufficiently prominent for investigation into the model sensitivity. This was done via single parameter perturbations (OAT analysis) with the same conditions as the main simulations ( $D_p = 50$  nm and  $T = 298.15$  K). Figs. S8, S9 and S10 show

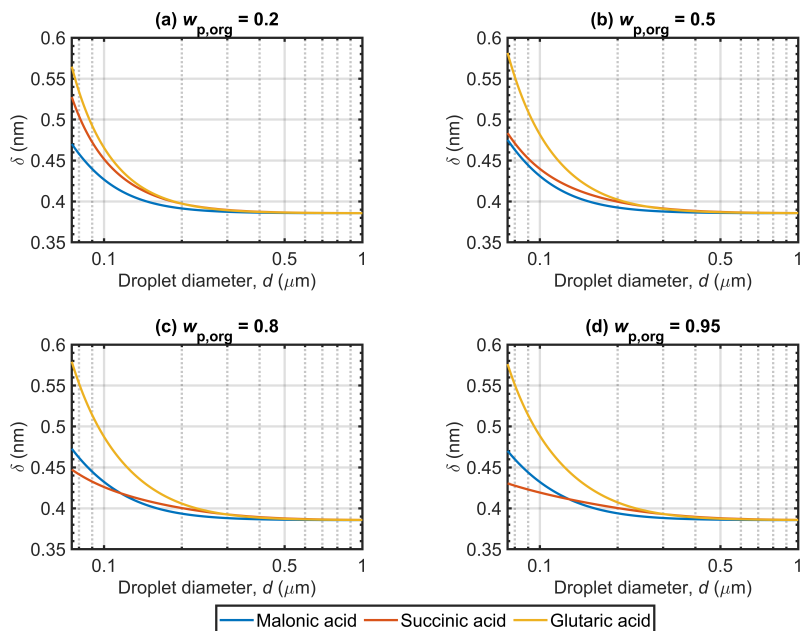


**Figure S7.** The droplet surface layer thickness along the Köhler curve predicted with the monolayer model of Malila and Prisle (2018) for  $D_p = 50$  nm at different organic mass fractions ( $w_{p,org}$ ) in the different panels for particles of ammonium sulphate mixed with malonic, succinic and glutaric acids.

**Table S4.** Compressed film model parameters used for in the calculations for the different organic compounds. All values were taken from Ruehl et al. (2016).

Compound	$A_0$ ( $\text{\AA}^2$ )	$m_\sigma$ ( $\text{mJ m}^{-2} \text{\AA}^{-2}$ )	$\log_{10} C_0$	$\sigma_{\min}$ ( $\text{mN m}^{-1}$ )
Malonic	71.2	1.13	-6.1	32.4
Succinic	76.9	1.04	-6.2	35.4
Glutaric	62	1.06	-7	30

the results of the analysis for malonic, succinic and glutaric acid Köhler curves. The Figs. contain 1%, 5% and 10% changes in parameters  $A_0$ ,  $\log_{10} C_0$ ,  $m_\sigma$  and  $\sigma_{\min}$  in shaded red areas around the baseline in black. These values were chosen based on the limits given in Ruehl et al. (2016) that vary between 1.6 - 8.5% depending on the compound and the parameter. The limits where the critical point moves to the second maxima is marked in blue line and a corresponding change in the other direction is also shown. The changes to the parameters in percentage are listed in Table S5. The changes were done as multipliers to the indicated parameters as for example  $A_0 \cdot X$  where  $X$  is the multiplier taken as  $(100\% \pm \Delta\%)/100$ . The values listed in Table S5 correspond to the  $\Delta\%$ .

There is a large difference in sensitivity between the compounds. The model is very robust with malonic and glutaric acid simulations, changing the critical point to the local maxima requiring significant changes in the parameters. Succinic acid simulation changes the location of the critical point with much smaller changes the other two compounds. This was to be expected as the local maxima is more prominent with succinic acid (Fig. S1).

The effect of the different parameters themselves can be observed in Figs S8, S9 and S10 for malonic, succinic and glutaric acids respectively. The molecular area  $A_0$  always influences the critical point, as well as the point where the surface tension

**Table S5.** Change in the compressed film model parameters (Table S4) needed to change the critical point to the second visible maxima. The changes were done as multipliers to the indicated parameters as for example  $A_0 \cdot X$  where  $X$  is the multiplier taken as  $(100\% \pm \Delta\%)/100$ . The tabulated values correspond to  $\Delta\%$ .

Compound	$A_0$ ( $\text{\AA}^2$ )	$m_\sigma$ ( $\text{mJ m}^{-2} \text{\AA}^{-2}$ )	$\log_{10} C_0$	$\sigma_{\min}$ ( $\text{mN m}^{-1}$ )
Malonic	-52.0%	-34.5%	+16.5% <sup>a</sup>	+9.1%
Succinic	-4.3%	-6.0%	+3.1% <sup>a</sup>	+4.2%
Glutaric	-44.7%	-36.6%	-	+21.9%

<sup>a</sup> The  $\log_{10} C_0$  itself is negative and this was calculated as  $\log_{10} C_0 \cdot X$  where  $X$  is a fraction  $(100\% + 9.1\%)/100$ , this is technically a smaller number

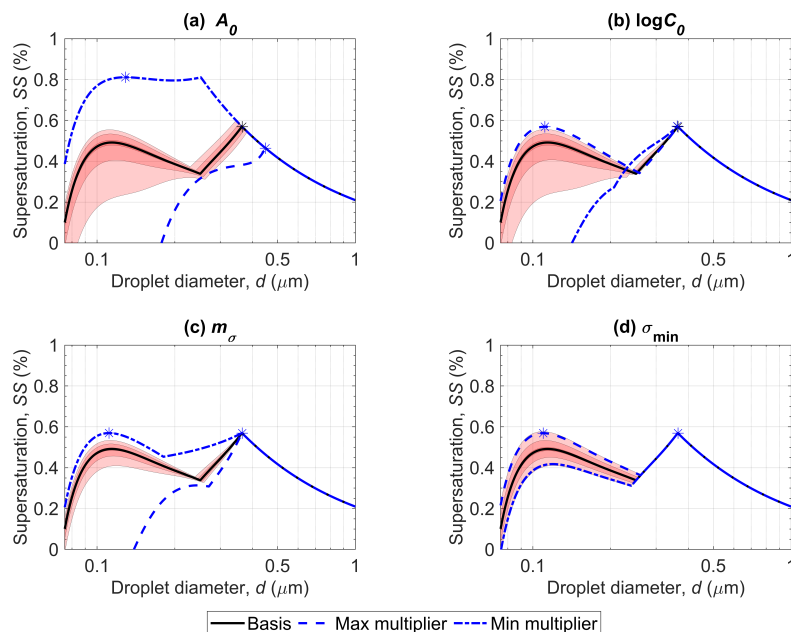


**Figure S8.** The sensitivity of the malonic acid supersaturation to changes in each of the compressed film model parameters. The red areas match 1%, 5% and 10% changes while the blue lines correspond to the change in the critical point listed in Table S5.

starts to increase. With malonic (Fig. S8) and succinic (Fig. S9) acid simulations, it also affects the first maxima while with glutaric acid only the second one excluding the large change needed to shift the critical point to the first maxima where the whole shape of the curve changes. Parameters  $\log_{10} C_0$  and  $m_\sigma$  affect the first maxima but does not seem to have a significant effect on the actual critical point before the maxima change. Glutaric acid simulation is an exception again,  $m_\sigma$  only has a small effect on the transition region where the surface tension changes. With  $\log_{10} C_0$ , the variation had no visible effect on the Köhler curve until very high changes. No change in the critical point to the first maxima was found. Of course,  $\sigma_{\min}$  itself has a clear effect but only during small droplet sizes, never affecting the critical point before it moves to the first maxima.

Simulations with glutaric acid (Fig. S10) could exhibit their unique behavior due to glutaric acid being the most surface active of the organic compounds used. The surface partitioning factor of glutaric acid is effectively equal to unity for all the 1-10% changes. Glutaric acid is also the most soluble in water out of the compounds investigated here.

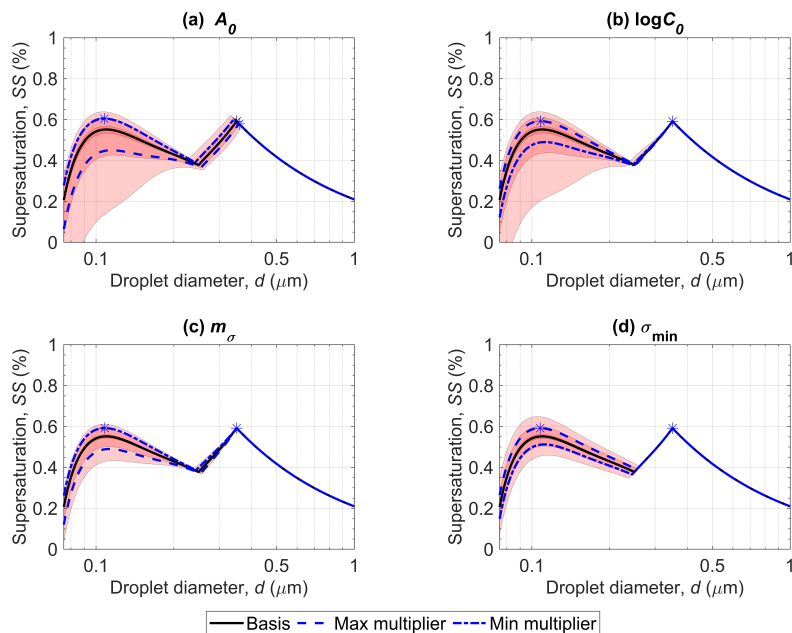


**Figure S9.** The sensitivity of the succinic acid supersaturation to changes in each of the compressed film model parameters. The red areas match 1%, 5% and 10% changes while the blue lines correspond to the change in the critical point listed in Table S5.

### S3 Thermodynamical data

#### 130 S3.1 Surface tension

The surface tension on the ternary system of water, organic and ammonium sulphate used with the monolayer (Malila and Prisle, 2018), Gibbs (Prisle et al., 2010) and bulk solution models is calculated with a parameterization into ternary system data by Booth et al. (2009). The data itself was measured at at 294.15 K. The equation used for the parameterization is an extension of the Szyszkowski-Langmuir equation (Szyszkowski, 1908; Meissner and Michaels, 1949; Tuckermann, 2007)

$$135 \quad \sigma = \sigma_w - ART \ln \left( 1 + \frac{x_{\text{org}}}{B} \right) + Cx_{\text{salt}} + Dx_{\text{salt}} \ln \left( 1 + \frac{x_{\text{org}}}{B} \right), \quad (\text{S9})$$

where the fitted parameters are  $A, B, C$  and  $D$ . The fit parameters for the three acids are listed in table S6 and during the simulations, the surface tension calculated by Eq.(S9) is used at 298.15 K and constrained by the pure compound as well as the binary surface tensions of water–salt and water–organic mixtures at the corresponding compositions.

140 The succinic and malonic acid binary fits are taken from Hyvärinen et al. (2006). For glutaric acid the equation is based on the measurements of Bzdek et al. (2016):

$$\sigma = \sigma_w - 4.6485 \cdot 10^{-3} \ln (1 + 9.8319c(x, T)), \quad (\text{S10})$$

where the function  $c$  converts glutaric mole fraction into molarity as

$$c = \frac{x\rho(x, T)}{(xM_{\text{org}} + (1-x)M_w)}, \quad (\text{S11})$$

where  $\rho$  is the density fit for binary mixture of water and glutaric acid (Cai et al., 2015).

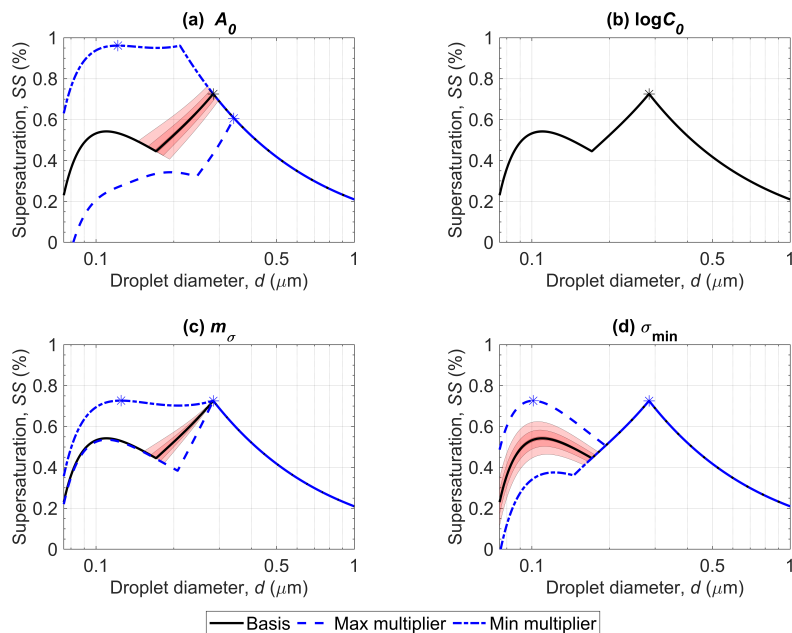


**Figure S10.** The sensitivity of the glutaric acid supersaturation to changes in each of the compressed film model parameters. The red areas match 1%, 5% and 10% changes while the blue lines correspond to the change in the critical point listed in Table S5.

145 The surface tension of the binary mixture of water and ammonium sulphate is calculated as

$$\sigma(c, T) = \sigma_w(T) + \frac{d\sigma}{dc}C, \quad (\text{S12})$$

where  $C$  is the salt mass concentration and

$$\frac{d\sigma}{dc} = 0.0179 \text{ mN/m L/g} = 2.3621 \text{ mN/m L/mol}. \quad (\text{S13})$$

150 The gradient was determined by combining data from Hyvärinen et al. (2005) and Aumann et al. (2010). The first point of Aumann et al. (2010) and the last two points of Hyvärinen et al. (2005) were ignored, and a LS fit was made into Eq. (S12) with the MATLAB (2019, 2020) function *fminsearch* at 298.15 K. The pure ammonium sulphate surface tension is estimated with Eq. (S12) with the mole fraction of ammonium sulphate set equal to unity. The conversion between mole fraction and mass concentration is calculated as

$$C = \frac{\rho x_{\text{salt}}}{M_w \left( \frac{x_{\text{salt}}}{M_w} + \frac{1-x_{\text{salt}}}{M_{\text{salt}}} \right)}, \quad (\text{S14})$$

155 where the aqueous ammonium sulphate density ( $\rho$ ) is calculated with the equation given by Tang and Munkelwitz (1994). The pure compound values and references are indicated in table S1 and the main article.

**Table S6.** The ternary surface tension parameters for water, ammonium sulphate and organic needed for Eq. (S9). The fits were done into ternary system data from Booth et al. (2009) at 294.15 K and the parameters have been rounded to four decimals.

Compound	$A$ (mol m <sup>-2</sup> )	$B$	$C$ (Jm <sup>-2</sup> )	$D$ (Jm <sup>-2</sup> )
Malonic	$3.2487 \cdot 10^{-6}$	0.0144	-0.0994	0.0242
Succinic	$6.5478 \cdot 10^{-7}$	$4.9852 \cdot 10^{-4}$	-0.3027	0.0285
Glutaric	$2.6222 \cdot 10^{-6}$	0.0032	-0.2271	0.0492

### S3.2 Density

The density of the ternary mixture is treated as a pseudo–binary ideal mixture of water-salt and organic:

$$x_{\text{salt}} = \frac{x_{\text{salt}}}{x_w + x_{\text{salt}}}, \quad (\text{S15})$$

$$160 \quad M = x_w M_w + x_{\text{salt}} M_{\text{salt}}, \quad (\text{S16})$$

$$x = x_w + x_{\text{salt}}, \quad (\text{S17})$$

and

$$\rho = \left( \frac{Mx}{\rho_{\text{salt},w} \sum_j (x_j M_j)} + \frac{M_{\text{org}} x_{\text{org}}}{\rho_{\text{org}} \sum_j (x_j M_j)} \right)^{-1}. \quad (\text{S18})$$

165 The binary ammonium sulphate–water mixture density ( $\rho_{\text{salt},w}$ ) is estimated from the binary fit Tang and Munkelwitz (1994). The pure compound values and references are indicated in table S1 and the main article. The binary densities of malonic acid and succinic acid are estimated according to Hyvärinen et al. (2006) while glutaric acid follows the fit recommended by Cai et al. (2015). These are used in case there is no salt present.

## References

- AIOMFAC-web: version 2.32, <https://aiomfac.lab.mcgill.ca>, accessed: 2020-08-19.
- 170 Aumann, E., Hildemann, L. M., and Tabazadeh, A.: Measuring and modeling the composition and temperature-dependence of surface tension for organic solutions, *Atmos. Environ.*, 44, 329–337, <https://doi.org/10.1016/j.atmosenv.2009.10.033>, 2010.
- Booth, A. M., Topping, D. O., McFiggans, G., and Percival, C. J.: Surface tension of mixed inorganic and dicarboxylic acid aqueous solutions at 298.15 K and their importance for cloud activation predictions, *Phys. Chem. Chem. Phys.*, 11, 8021–8028, <https://doi.org/10.1039/B906849J>, 2009.
- 175 Bzdek, B. R., Power, R. M., Simpson, S. H., Reid, J. P., and Royall, C. P.: Precise, contactless measurements of the surface tension of picolitre aerosol droplets, *Chem. Sci.*, 7, 274–285, <https://doi.org/10.1039/C5SC03184B>, 2016.
- Cai, C., Stewart, D. J., Reid, J. P., Zhang, Y.-h., Ohm, P., Dutcher, C. S., and Clegg, S. L.: Organic Component Vapor Pressures and Hygroscopicities of Aqueous Aerosol Measured by Optical Tweezers, *J. Phys. Chem. A*, 119, 704–718, <https://doi.org/10.1021/jp510525r>, PMID: 25522920, 2015.
- 180 CRC Handbook: CRC Handbook of Chemistry and Physics, 1st Student Edition, CRC Press, Boca Raton, FL., 1988.
- Forestieri, S. D., Staudt, S. M., Kuborn, T. M., Faber, K., Ruehl, C. R., Bertram, T. H., and Cappa, C. D.: Establishing the impact of model surfactants on cloud condensation nuclei activity of sea spray aerosol mimics, *Atmos. Chem. Phys.*, 18, 10985–11005, <https://doi.org/10.5194/acp-18-10985-2018>, 2018.
- Hyvärinen, A.-P., Raatikainen, T., Laaksonen, A., Viisanen, Y., and Lihavainen, H.: Surface tensions and densities of H<sub>2</sub>SO<sub>4</sub> + NH<sub>3</sub> + water solutions, *Geophys. Res. Lett.*, 32, 1–5, <https://doi.org/10.1029/2005GL023268>, 2005.
- 185 Hyvärinen, A.-P., Lihavainen, H., Gaman, A., Vairila, L., Ojala, H., Kulmala, M., and Viisanen, Y.: Surface Tensions and Densities of Oxalic, Malonic, Succinic, Maleic, Malic, and cis-Pinonic Acids, *J. Chem. Eng. Data*, 51, 255–260, <https://doi.org/10.1021/je050366x>, 2006.
- Malila, J. and Prisle, N. L.: A Monolayer Partitioning Scheme for Droplets of Surfactant Solutions, *J. Adv. Model. Earth Syst.*, 10, 3233–3251, <https://doi.org/10.1029/2018MS001456>, 2018.
- 190 MATLAB: version 9.6.0.1072779 (R2019a), The MathWorks Inc., Natick, Massachusetts, 2019.
- MATLAB: version 9.8.0.1323502 (R2020a), The MathWorks Inc., Natick, Massachusetts, 2020.
- Meissner, H. P. and Michaels, A. S.: Surface Tensions of Pure Liquids and Liquid Mixtures, *Ind. Eng. Chem.*, 41, 2782–2787, <https://doi.org/10.1021/ie50480a028>, 1949.
- Ovadnevaite, J., Zuend, A., Laaksonen, A., Sanchez, K. J., Roberts, G., Ceburnis, D., Decesari, S., Rinaldi, M., Hodas, N., Facchini, M. C., Seinfeld, J. H., and O’Dowd, C.: Surface tension prevails over solute effect in organic-influenced cloud droplet activation, *Nature*, 546, 637–641, <https://doi.org/10.1038/nature22806>, 2017.
- 195 Prisle, N. L.: Cloud Condensation Nuclei Properties of Organic Aerosol Particles: Effects of Acid Dissociation and Surfactant Partitioning, Master’s thesis, University of Copenhagen, Copenhagen, 2006.
- Prisle, N. L., Raatikainen, T., Laaksonen, A., and Bilde, M.: Surfactants in cloud droplet activation: mixed organic-inorganic particles, *Atmos. Chem. Phys.*, 10, 5663–5683, <https://doi.org/10.5194/acp-10-5663-2010>, 2010.
- 200 Prisle, N. L., Dal Maso, M., and Kokkola, H.: A simple representation of surface active organic aerosol in cloud droplet formation, *Atmos. Chem. Phys.*, 11, 4073–4083, <https://doi.org/10.5194/acp-11-4073-2011>, 2011.
- Ruehl, C. R., Davies, J. F., and Wilson, K. R.: An interfacial mechanism for cloud droplet formation on organic aerosols, *Science*, 351, 1447–1450, <https://doi.org/10.1126/science.aad4889>, 2016.
- 205 Szyszkowski, B.: Experimentelle Studien über kapillare Eigenschaften der wässerigen Lösungen von Fettsäuren., *Zeitschrift für Physikalische Chemie*, 64U, 385–414, <https://doi.org/doi:10.1515/zpch-1908-6425>, 1908.
- Tang, I. N. and Munkelwitz, H. R.: Water activities, densities, and refractive indices of aqueous sulfates and sodium nitrate droplets of atmospheric importance, *J. Geophys. Res. D: Atmos.*, 99, 18 801–18 808, <https://doi.org/10.1029/94JD01345>, 1994.
- Tuckermann, R.: Surface tension of aqueous solutions of water-soluble organic and inorganic compounds, *Atmos. Environ.*, 41, 6265 – 6275, <https://doi.org/https://doi.org/10.1016/j.atmosenv.2007.03.051>, 2007.
- 210 Vanhanen, J., Hyvärinen, A.-P., Anttila, T., Raatikainen, T., Viisanen, Y., and Lihavainen, H.: Ternary solution of sodium chloride, succinic acid and water; surface tension and its influence on cloud droplet activation, *Atmos. Chem. Phys.*, 8, 4595–4604, <https://doi.org/10.5194/acp-8-4595-2008>, 2008.
- Young, K. C. and Warren, A. J.: A Reexamination of the Derivation of the Equilibrium Supersaturation Curve for Soluble Particles, *J. Atmos. Sci.*, 49, 1138–1143, [https://doi.org/10.1175/1520-0469\(1992\)049<1138:AROTDO>2.0.CO;2](https://doi.org/10.1175/1520-0469(1992)049<1138:AROTDO>2.0.CO;2), 1992.
- 215